Universal origin of heavy elements

Jose Orce (jnorce@uwc.ac.za)
University of the Western Cape https://orcid.org/0000-0003-1699-1761

Balaram Dey
Bankura University

Cebo Ngwetsheni
University of the Western Cape

Brenden Lesch
University of the Western Cape

Andile Zulu
University of the Western Cape

Srijit Bhattacharya
Barasat Govt. College

Deepak Pandit
Variable Energy Cyclotron Centre

Sumeera Gopal
University of Zululand

Siphamandla Khumalo
University of Zululand

Sifiso Mngonyama
University of Zululand

Gift Mthethwa
University of Zululand

Yandisa Ndala
University of the Western Cape

Asive Ndingi
University of the Western Cape

Ignasio Wakudyanaye
University of the Western Cape

Physics Article

Keywords: heavy elements, Bethe-Weizsacker semi-empirical mass formula, binding energy, universal origin

Posted Date: May 5th, 2021

DOI: https://doi.org/10.21203/rs.3.rs-440633/v1

Universal origin of heavy elements

José Nicolás Orce[1,+], Balaram Dey[2], Cebo Ngwetsheni[1], Brenden Lesch[1], Andile Zulu[1], Srijit Bhattacharya[3], Sumeera Gopal[4], Siphamandla Khumalo[4], Sifiso Mngonyama[4], Gift Mthethwa[4], Yandisa Ndala[1], Asive Ndingi[1], Deepak Pandit[5,6], Ignasio Wakudyanaye[1]

[1]*Department of Physics & Astronomy, University of the Western Cape, P/B X17, Bellville, ZA-7535 South Africa*

[2]*Department of Physics, Bankura University, Bankura-722155, West Bengal, India*

[3]*Department of Physics, Barasat Govt. College, Barasat, West Bengal-700124, India*

[4]*Department of Physics & Engineering, University of Zululand, P/B X1001, KwaDlangezwa 3886, South Africa*

[5] *Variable Energy Cyclotron Centre, 1/AF-Bidhannagar, Kolkata-700064, India*

[6]*Homi Bhabha National Institute, Training School Complex, Anushaktinagar, Mumbai 400094, India*

[+]*jnorce@uwc.ac.za*

The abundance of heavy elements through the rapid neutron capture process or r-process is intimately related to the competition between neutron capture and β decay rates, which ultimately depends on the binding energy of atomic nuclei. The well-known Bethe-Weizsäcker semi-empirical mass formula[1,2] describes the binding energy of ground states in nuclei with temperatures of $T \approx 0$ MeV, where the nuclear symmetry energy saturates between $23-26$ MeV. Here we find a larger saturation energy of ≈ 30 MeV for nuclei at $T \approx 0.7-1.3$ MeV,

which corresponds to the typical temperatures where seed elements are created during the cooling down of the ejecta following neutron-star mergers[3] and collapsars[4]. This large symmetry energy yields a reduction of the binding energy per nucleon for neutron-rich nuclei; hence, the close in of the neutron dripline, where nuclei become unbound. This finding constrains exotic paths in the nucleosynthesis of heavy elements – as supported by microscopic calculations of radiative neutron-capture rates [5] – and further supports the universal origin of heavy elements, as inferred from the abundances in extremely metal-poor stars and meteorites.

Acknowledgments This work was supported by the National Research Foundation (NRF) of South Africa under Grant 93500 and by the MANuS/MatSci Honours/MSc programme also funded by the NRF.

Competing Interests The authors declare that they have no competing financial interests.

Correspondence Correspondence and requests for materials should be addressed to jnorce@uwc.ac.za.

The binding energy of a nucleus with Z protons and N neutrons can be described by the well-known Bethe-Weizsäcker semi-empirical mass formula (SEMF) [1,2],

$$\begin{aligned} B(Z,A) &= a_v A - a_s A^{2/3} - a_c Z(Z-1)A^{-1/3} \\ &- a_{sym}\frac{(A-2Z)^2}{A} \pm a_p A^{-3/4}, \end{aligned} \tag{1}$$

where $A = Z+N$ is the mass number and a_v, a_s, a_c, a_{sym} and a_p are the volume, surface, Coulomb, symmetry energy and pairing coefficients, respectively. The symmetry energy, $a_{sym}(A)(N -$

$Z)^2/A$, reduces the total binding energy $B(Z, A)$ of a nucleus as the neutron-proton asymmetry becomes larger, i.e. for $N \gg Z$, and yields the typical negative slope of the binding energy curve [6] for $A > 62$. It is divided by A to reduce its importance for heavy nuclei, and it depends on the mass dependency of $a_{sym}(A)$. Its convergence for heavy nuclei establishes the frontiers of the neutron dripline for particle-unbound nuclei and eventually leads to the disappearance of protons at extreme nuclear densities [7].

Additionally, $a_{sym}(A)$ is relevant to understanding neutron skins [8], the effect of three-nucleon forces [9] and – through the equation of state (EoS) – supernovae cores, neutron stars and binary mergers [10–12]. The latter are the first known astrophysical site where heavy elements are created through the rapid neutron-capture or r-process [5,13]. The identification of heavy elements in neutron star mergers is supported by the short duration gamma-ray bursts via their infrared afterglow [14] – only understood by the opacities of heavy nuclei – as well as blueshifted Sr II absorption lines [15], following the expansion speed of the ejecta gas at $v = 0.1 - 0.3\ c$. Mergers are expected to be the only source for the creation of elements above lead and bismuth, as inferred from the very scarce abundance of actinides in the solar system [16]. Other potential sources of heavy elements involve different types of supernova (e.g. collapsars [4] – the supernova-triggering collapse of rapidly rotating massive stars – and type-II supernova [5]), which need to be considered to elucidate the universality of r-process abundances [17] in extremely metal-poor stars [18].

It is the motivation of this work to understanding the limits of the neutron dripline and heavy-element production through the r-process by investigating $a_{sym}(A)$ at different temperatures using

available data; namely, photo-absorption cross sections, binding energies and giant dipole resonances. Generally, $a_{sym}(A)$ is parametrized using the leptodermous approximation of Myers and Swiatecki, where $A^{-1/3} \ll 1$ [19],

$$a_{sym}(A) = S_v \left(1 - \frac{S_s}{S_v} A^{-1/3}\right), \tag{2}$$

which considers the modification of the volume symmetry energy, S_v, by the surface symmetry energy S_s.

The giant dipole resonance (GDR) represents the main contribution to the absorption and emission of electromagnetic radiation (photons) in nuclei [20]. The dynamics of this quantum collective excitation is characterized by the inter-penetrating motion of proton and neutron fluids out of phase [21], which results from the density-dependent symmetry energy, $a_{sym}(A)(\rho_{_N} - \rho_{_Z})^2/\rho$, acting as a restoring force [20]; where $\rho_{_N}$, $\rho_{_Z}$ and $\rho = \rho_{_N} + \rho_{_Z}$ are the neutron, proton and total density, respectively, which spread uniformly throughout the nucleus.

The ratio of the induced dipole moment to an applied constant electric field yields the static nuclear polarizability, α. Using the hydrodynamic model and assuming inter-penetrating proton and neutron fluids with a well-defined nuclear surface of radius $R = r_{_0} A^{1/3}$ fm and $\rho_{_Z}$ as the potential energy of the liquid drop, Migdal [21] obtains the following relation between the static nuclear polarizability, α, and a_{sym},

$$\alpha = \frac{e^2 R^2 A}{40 a_{sym}} = 2.25 \times 10^{-3} A^{5/3} \text{fm}^3, \tag{3}$$

where $r_{_0} = 1.2$ fm, $e^2 = 1.44$ MeV fm in the c.g.s. system, and a constant value of $a_{sym} = 23$ MeV was utilized.

Alternatively, α can be calculated for the ground states of nuclei using second-order perturbation theory [22] following the sum rule,

$$\alpha = 2e^2 \sum_n \frac{\langle i \parallel \hat{E1} \parallel n\rangle\langle n \parallel \hat{E1} \parallel i\rangle}{E_\gamma} \quad (4)$$

$$= \frac{e^2\hbar^2}{M} \sum_n \frac{f_{in}}{E_\gamma^2} = \frac{\hbar c}{2\pi^2} \int_0^\infty \frac{\sigma_{total}(E_\gamma)}{E_\gamma^2}\, dE_\gamma \quad (5)$$

$$= \frac{\hbar c}{2\pi^2}\sigma_{-2}, \quad (6)$$

where E_γ is the γ-ray energy corresponding to a transition connecting the ground state $|i\rangle$ and an excited state $|n\rangle$, M the nucleon mass, f_{in} the dimensionless oscillator strength for $E1$ transitions [22] and σ_{-2} the second moment of the total electric-dipole photo-absorption cross section,

$$\sigma_{-2} = \int_0^\infty \frac{\sigma_{total}(E_\gamma)}{E_\gamma^2}\, dE_\gamma, \quad (7)$$

where $\sigma_{total}(E_\gamma)$ is the total photo-absorption cross section, which generally includes $(\gamma, n) + (\gamma, pn) + (\gamma, 2n) + (\gamma, 3n)$ photoneutron and scarcely available photoproton cross sections [23], in competition in the GDR region [24,26]. By comparing Eqs. 3 and 6, a mass-dependent symmetry energy, a_{sym}(A), is extracted in units of MeV,

$$a_{sym}(A) = \frac{e^2R^2\pi^2A}{20\,\hbar c\,\sigma_{-2}} \approx 5.2 \times 10^{-3}\,\frac{A^{5/3}}{\sigma_{-2}}. \quad (8)$$

Empirical evaluations reveal that σ_{-2} can also be approximated by $\sigma_{-2} = 2.4\kappa A^{5/3}$, where the dipole polarizability parameter κ measures GDR deviations between experimental and hydrodynamic model predictions [27].

Figure 1 shows the distribution of $a_{sym}(A)$ for the ground state of stable isotopes, along the nuclear landscape, determined by empirical σ_{-2} values. The contribution of (γ, p) cross sections

are evident in light nuclei, which significantly reduces the symmetry energy. For heavy nuclei, (γ, n) cross sections are dominant because of the higher Coulomb barrier. A fit to the data using Eq. 2 (solid line) yields $a_{sym}(A) = 31.72\left(1 - 1.31A^{-1/3}\right)$ MeV, with an RMS deviation of 22% [?]. Unfortunately, (γ, p) cross-section data are very scarce, which directly affects the $a_{sym}(A)$ trend in Fig. 1. A similar attempt to characterize $a_{sym}(A)$ can be extracted from a free fit to the available total nuclear photo-absorption data [28], which yields $a_{sym}(A) = 25.6\left(1 - 1.66A^{-1/3}\right)$ MeV.

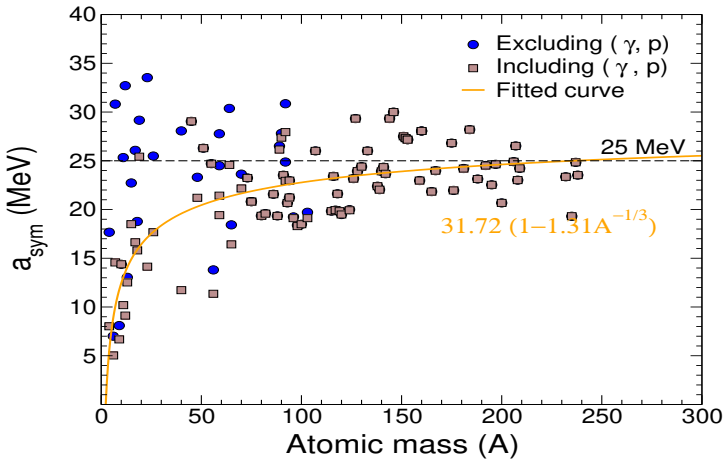

Figure 1: Symmetry energy coefficient, $a_{sym}(A)$, of finite nuclei as a function of mass number A extracted from the experimental σ_{-2} values [36,37], as given in Eq. 8 and fitted (solid line) by Eq. 2.

From a global fit to the binding energies of isobaric nuclei with $A \geq 10$ [29], extracted from the 2012 atomic mass evaluation [30], Tian and co-workers determined $a_{sym}(A) = 28.32\left(1 - 1.27A^{-1/3}\right)$ MeV, with $S_v \approx 28.32$ MeV being the bulk symmetry energy coefficient and $\frac{S_s}{S_v} \approx 1.27$ the surface-to-volume ratio. Similar coefficients are calculated in Refs. [10,31]. Within this approach, the extraction of $a_{sym}(A)$ only depends on the Coulomb energy term in the SEMF and shell effects [32] – which are both included [29] – and $a_{sym}(A)$ saturates at around 23 MeV. This description of $a_{sym}(A)$

has been used to explain the enhanced σ_{-_2} values observed for low-mass nuclei [?].

The symmetry energy $a_{sym}(A)$ is the fundamental parameter that characterizes the energy of the GDR, $E_{_{GDR}}$, within the Steinwedel-Jensen (SJ) model of proton and neutron compressible fluids moving within the rigid surface of the nucleus [33]. Danos improved the SJ model by including the GDR width, $\Gamma_{_{GDR}}$ [20,34] in the second-sound hydrodynamic model [20,34], where $E_{_{GDR}}$ and $\Gamma_{_{GDR}}$ are related to $a_{sym}(A)$ as [26],

$$\begin{aligned} a_{sym}(A) &= \frac{MA^2}{8\hbar^2K^2NZ}\frac{E^2_{_{GDR}}}{1-\left(\frac{\Gamma_{GDR}}{2E_{_{GDR}}}\right)^2} \\ &\approx 1\times10^{-3}\Big(\frac{A^{8/3}}{NZ}\Big)\frac{E^2_{_{GDR}}}{1-\left(\frac{\Gamma_{GDR}}{2E_{_{GDR}}}\right)^2}, \end{aligned} \tag{9}$$

where K is the real eigenvalue of $\bigtriangledown^2\rho_{_Z}+K^2\rho_{_Z}=0$, with the boundary condition $(\hat{\mathbf{n}}\bigtriangledown\rho_{_Z})_{_{surface}}=0$, and has a value of $KR=2.082$ for a spherical nucleus [35]. For quadrupole deformed nuclei with an eccentricity of $a^2-b^2=\epsilon R^2$, where a and b are the half axes and ϵ the deformation parameter, the GDR splits into two peaks with similar values of Ka and $Kb\approx2.08$ [34]. Henceforth, we propose the symmetrized relation for deformed nuclei,

$$a_{sym}(A) = 1\times10^{-3}\Big(\frac{A^{8/3}}{NZ}\Big)\frac{E_{_{GDR_1}}E_{_{GDR_2}}}{1-\frac{\Gamma_{GDR_1}\Gamma_{GDR_2}}{4E_{_{GDR_1}}E_{_{GDR_2}}}}. \tag{10}$$

The GDR cross-section data for each nucleus was obtained from the EXFOR and ENDF databases [36,37] and fitted with one or two Lorentzian curves to extract $E_{_{GDR}}$ and $\Gamma_{_{GDR}}$, as shown e.g. in Fig. 2 for ^{208}Pb. The data set for each nucleus was selected based on the number of data

points, experimental method and energy range. In this work, the maximum integrated γ-ray energy, E_γ^{max}, was in the range 20–50 MeV, therefore excluding contributions resulting from high energy effects such as pion exchange and other meson resonances. The resulting distribution of $a_{sym}(A)$ is shown in the left panel of Fig. 3, which presents saturation at around 26 MeV for heavy nuclei. It is reassuring that the two methods based on photo-absorption cross-section data — namely $a_{sym}(A)$ extracted from σ_{-2} values and parameters of GDRs built on ground states – present similar trends.

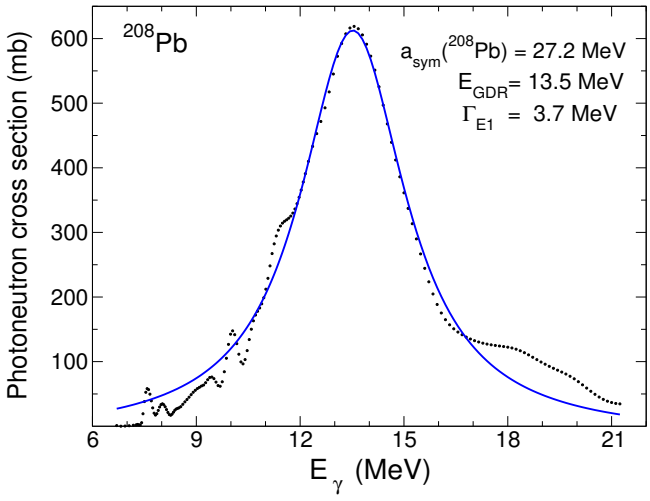

Figure 2: A Lorentzian fit to GDR data extracted for ^{208}Pb [36,37].

Data obtained from GDR parameters can also be fitted to Eq. 2, which yields $a_{sym}(A) = 33.09\left(1 - 1.39A^{-1/3}\right)$ MeV, with an RMS deviation of 33%. Larger values of $S_v = 42.8$ and $S_s = 89.9$ were determined by Berman using Eq. 9 for 29 nuclei ranging from $A = 75$ to 209 [38]. Furthermore, Berman argued that assuming a surface binding energy coefficient of $a_{_S} = 20$ MeV in the SEMF, the large symmetry to surface energy ratio, $S_s/a_{_S} = 4.5$, favors – as a result of a steeper slope of the binding energy curve for heavy nuclei – a close-in neutron dripline for heavy elements; hence, constraining the reaction network that produces heavy elements by the r-process

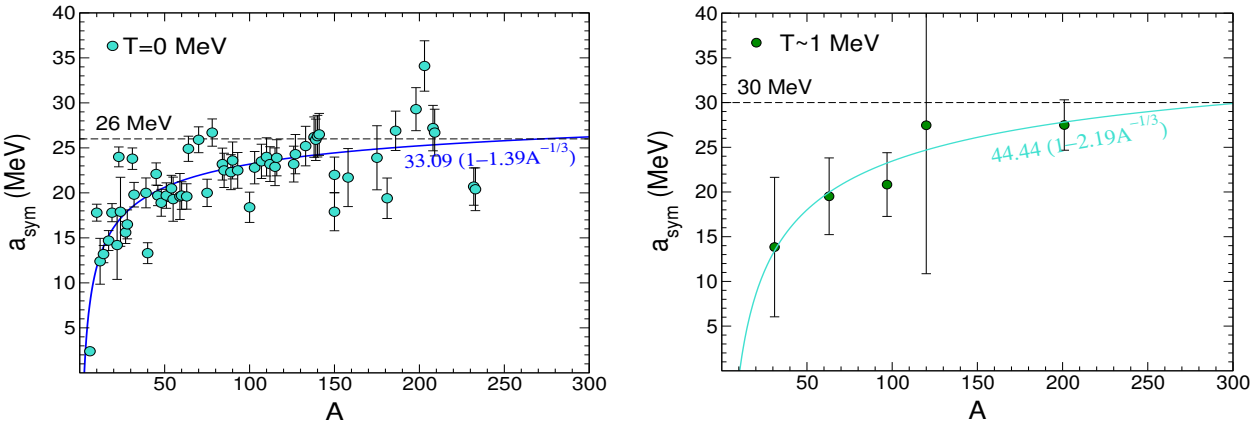

Figure 3: (Color online) Symmetry energy coefficient, $a_{sym}(A)$, of finite nuclei as a function of mass number A extracted from GDRs built on ground states ($T = 0$) (left panel) and excited states ($T \approx 1$ MeV) (right panel) using Eqs. 9 and 10.

in neutron mergers and supernovae. Using our value of $S_s = 46$ and $a_S = 20$ MeV, a more reasonable ratio of $S_s/a_S = 2.3$ is determined. Slightly smaller values of $a_S \approx 17$ MeV are also found in the literature [6,31], yielding $S_s/a_S = 2.7$.

Furthermore, it is interesting to investigate the behavior of $a_{sym}(A)$ using the available information on GDRs built on excited states, below the critical temperatures and spins where the GDR width starts broadening; i.e. for moderate average temperatures of $T \lessapprox T_c = 0.7 + 37.5/A$ MeV and spins J below the critical angular momentum $J \lessapprox J_c = 0.6A^{5/6}$. In fact, similar centroid energies, E^{exc}_{GDR}, and resonance strengths, S^{exc}_{GDR} – relative to the Thomas–Reiche–Kuhn $E1$ sum rule [22] – to those found for the ground-state counterparts [24,25] indicate a common physical origin for all GDRs, in concordance with the Brink–Axel hypothesis that assumes that a GDR can be built on every state in a nucleus [39,40].

Applying again Eqs. 9 and 10, the right panel of Fig. 3 shows $a_{sym}(A)$ values for GDRs built on excited states in ^{31}P [41], ^{63}Cu [42], ^{97}Tc [43], ^{120}Sn [44] and ^{201}Tl [45], with an average temperature of $T \approx 1$ MeV and below J_c. Surprisingly, although the trend is not as well defined as for cold nuclei, $a_{sym}(A)$ seems to saturate at a higher energy than previously observed for cold nuclei at $T = 0$ MeV. Moreover, $a_{sym}(A)$ for a particular nucleus does not change with temperature between the upper ($T \approx 1.3$ MeV) and lower ($T \approx 0.7$ MeV) experimental values [42,43,45]. A saturation energy of $a_{sym}(A) = 30$ MeV yields larger values of $S_v = 44.44$, $S_s = 97.32$ and $S_s/a_s = 4.87$ (again for $a_s = 20$ MeV), which clearly affects nucleosynthesis of heavy elements via the r-process during the cooling down of the ejecta. More experimental data for GDRs built on excited states are crucially needed in order to understand the nature of the symmetry energy as a function of temperature; particularly there are no data for $A < 30$ and $T < 0.7$ MeV.

Lighter or heavier seed nuclei are generally produced depending on the density and temperature of the ejecta gas. Assuming nuclear-statistical equilibrium – when forward and reverse reactions are balanced – abundances follow a Maxwell-Boltzmann distribution where lighter seed nuclei are favoured at very high temperatures ($\propto kT^{-3/2(A-1)}$) and heavier nuclei are favoured at very high densities ($\propto \rho^{A-1}$), as those found in the ejecta of neutron-star mergers [3]. At temperatures below $T = 1$ MeV (or 1.2×10^{10} K), seed nuclei are produced before charge reactions freeze out – impeded by the Coulomb barrier – at about $T \approx 0.3$ MeV (or 3×10^9 K). Thereafter, heavy nuclei are produced through subsequent neutron capture until neutron reactions freeze out – as neutrons are finally consumed – at a few 10^8 K.

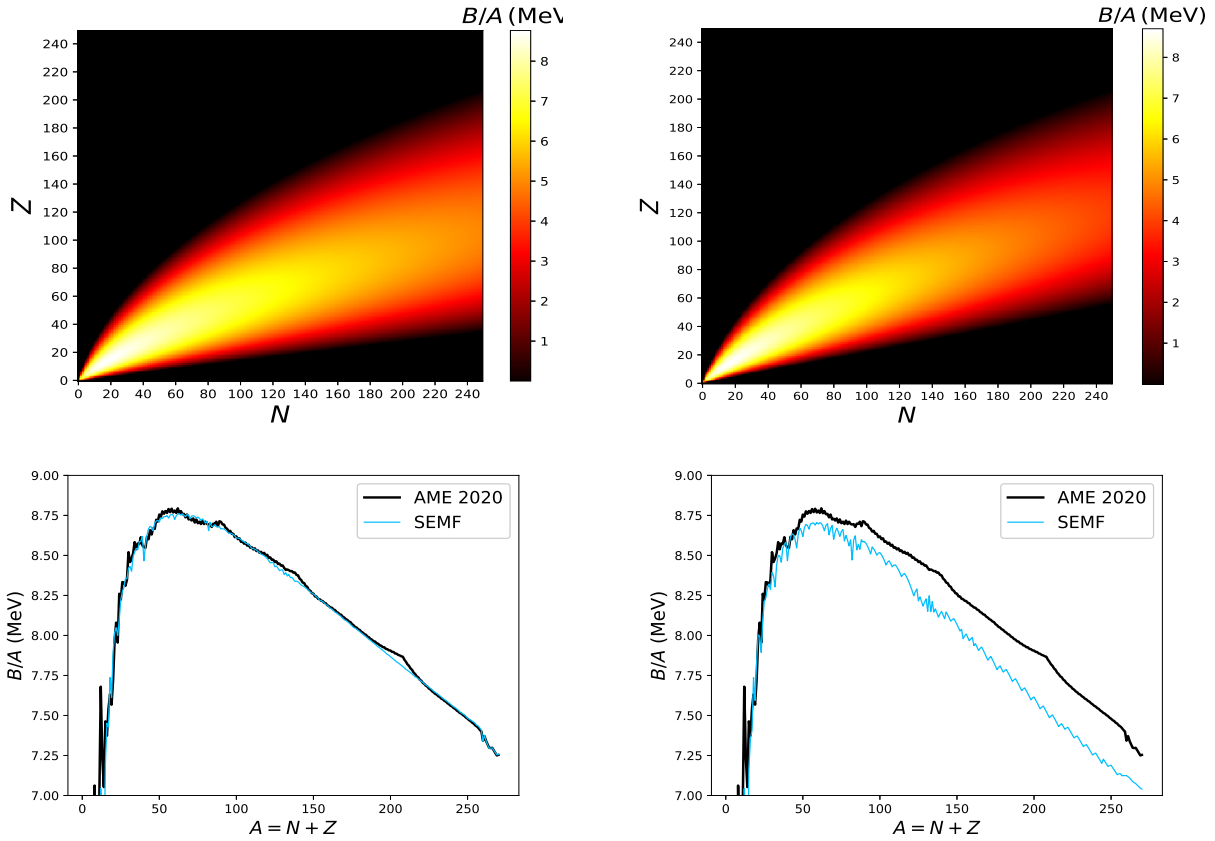

Figure 4: (Color online) Nuclear charts (top panels) and binding energy curves (bottom panels) showing average binding energies per nucleon using the Bethe-Weizsäcker SEMF for $a_{sym} = 23$ MeV (left) and $a_{sym} = 30$ MeV (right). Atomic masses in the bottom panels are extracted from the 2020 atomic mass evaluation (AME 2020) [46].

Finally, the effects from the larger symmetry energy determined in this work are shown in Fig. 4, which shows the corresponding nuclear charts (top) and binding energy curves (bottom) using $a_{sym} = 23$ MeV (left) and 30 MeV (right), respectively. The nuclear chart determined using $a_{sym} = 30$ MeV illustrates a substantial close-in of the neutron dripline, as a result of the decreasing binding energy per nucleon in neutron-rich nuclei. These findings support the rapid drop of

the neutron capture rates at increasing neutron excesses inferred from Goriely's microscopic calculations at $T = 1.5 \times 10^9$ K [5]; hence, constraining exotic r-process paths close to the neutron dripline and plausibly explaining the universality of r-process abundances inferred from extremely metal-poor stars.

1. von Weizsäcker, C. F. Zur Theorie der Kernmassen. Z. Phys. **96** (1935) 431.

2. Bethe, H. A. & Bacher, R. F. Stationary States of Nuclei. Rev. Mod. Phys. **8** (1936) 82.

3. Thielemann, F. -K., Eichler, M., Panov, I.V. & Wehmeyer, B. Neutron Star Mergers and Nucleosynthesis of Heavy Elements. Annu. Rev. Nucl. Part. Sci. **67** (2017) 25374.

4. Siegel, D. M., Barnes, J. & Metzger, B. D. Collapsars as a major source of r-process elements. Nature **569** (2019) 241244.

5. Goriely, S. The r-process nucleosynthesis: a continued challenge for nuclear physics. Nucl. Phys. A **718** (2003) 287c-294c.

6. Krane, K. S. *Introductory Nuclear Physics*, Wiley (1987).

7. Kutschera, M. Nuclear symmetry energy and structure of dense matter in neutron stars. Phys. Lett. B **340** (1994) 1-5.

8. Piekarewicz, J. *et al.* Electric dipole polarizability and the neutron skin. Phys. Rev. C **85** (2012) 041302(R).

9. Hebeler, K. & Schwenk, A. Symmetry energy, neutron skin, and neutron star radius from chiral effective field theory interactions. Eur. Phys. J. A **50** (2014) 11.

10. Steiner, A. W., Prakash, M., Lattimer, J. M. & Ellis, P. J. Isospin asymmetry in nuclei and neutron stars. Phys. Rep. **411** (2005) 325.

11. Latimer, J. M. Symmetry energy in nuclei and neutron stars. Nucl. Phys. A **928** (2014) 276.

12. Pearson, J. M., Chamel, N., Fantina, A. F. & Goriely, S. Symmetry energy: nuclear masses and neutron stars. Eur. Phys. J. A **50** (2014) 43.

13. Cowan, J. J., Sneden, C., Lawler, J. E., Aprahamian, A., Wiescher, M., Langanke, K., Martínez-Pinedo, G. & Thielemann, F. -K. Origin of the heaviest elements: The rapid neutron-capture process. Rev. Mod. Phys. **93** (2021) 015002.

14. Metzger, B. D. Kilonova. Living Reviews in Relativity **20** (2017) 3.

15. Watson, D. *et al.* Identification of strontium in the merger of two neutron stars. Nature **574** (2019) 497.

16. Bartos, I. & Marka, S. A nearby neutron-star merger explains the actinide abundances in the early Solar System. Nature **569** (2019) 8588.

17. Qian, Y.-Z. Supernovae versus neutron star mergers as the major r-process sources. Astrophys. J. **534** (2000) L67.

18. Christlieb, N. *et al*. A stellar relic from the early Milky Way. Nature **419** (2002) 904906.

19. Myers, W. D. & Swiatecki, W. J. Average nuclear properties. Ann. Phys. **55** (1969) 395.

20. Berman, B. L. & Fultz, S. C. Measurements of the giant dipole resonance with monoenergetic photons. Rev. Mod. Phys. **47** (1975) 713.

21. Migdal, A. B. Quadrupole and dipole gamma-radiation of nuclei. J. Exptl. Theoret. Phys. U.S.S.R. **15** (1945) 81.

22. Levinger, J. S. *Nuclear Photo-Disintegration*. Oxford University Press, Oxford (1960).

23. Kawano, T. *et al.*. IAEA Photonuclear Data Library 2019. Nucl. Data Sheets **163** (2020) 109-162.

24. Snover, K. A. Giant Resonances in Excited Nuclei. Ann. Rev. Nucl. Part. Sci. **36** (1986) 545.

25. Gaardhøje, J. J. Nuclear Structure at High Excitation Energy Studied with Giant Resonances. Annu. Rev. Nucl. Part. Sci. **42** (1992) 483.

26. Bergere, R. Lecture Notes in Physics **61**, *Photonuclear Reactions I*, (Springer-Verlag, 1977).

27. Orce, J. N. Polarizability effects in atomic nuclei. Int. J. Mod. Phys. E **29** (2020) 2030002.

28. von Neumann-Cosel, P. Comment on"New formulas for the (-2) moment of the photoabsorption cross section, σ_{-2}". Phys. Rev. C **93** (2016) 049801.

29. Tian, J., Cui, H., Zheng, K. & Wang, N. Effect of Coulomb energy on the symmetry energy coefficients of finite nuclei. Phys. Rev. C **90** (2014) 024313.

30. Wang, M., Audi, G., Wapstra, A. H. & Kondev, F. G.. The AME2016 atomic mass evaluation (II). Chin. Phys. C **36** (2012) 1603.

31. Danielewicz, P. Surface Symmetry Energy. Nucl. Phys. A **727** (2003) 233.

32. Koura, H., Tachibana, T., Uno, M. & Yamada, M. Nuclidic Mass Formula on a Spherical Basis with an Improved Even-Odd Term. Prog. Theor. Phys. **113** (2005) 305.

33. Steinwedel, H., Jensen, J. H. D. & Jensen, P. Nuclear Dipole Vibrations. Phys. Rev. **79** (1950) 1019.

34. Danos, M. On the long-range correlation model of the photonuclear effect. Nucl. Phys. **5** (1958) 23.

35. Lord Rayleigh, *The Theory of Sound*, second edition (MacMillan Co., London, 1896) Chapter XVII.

36. EXFOR: Experimental Nuclear Reaction Data. https://www-nds.iaea.org/exfor/exfor.htm

37. ENDF: Evaluated Nuclear Data File. https://www-nds.iaea.org/exfor/endf.htm (iaea.org)

38. Berman, B. L. Mass variation of the nuclear symmetry energy. *Proceedings of the International Conference on Photonuclear Reactions and Applications, Pacific Grove, California*, ed. by B. L. Berman (Lawrence Livermore Laboratory, Livermore) (1973) 569.

39. Brink, D. Some aspects of the interaction of light with matter. Doctoral thesis, Oxford University, 1955 (unpublished).

40. Axel, P. Electric Dipole Ground-State Transition Width Strength Function and 7-Mev Photon Interactions. Phys. Rev. **126** (1962) 671.

41. Mondal, D. *et al.* Study of giant dipole resonance in hot rotating light mass nucleus ^{31}P. Phys. Lett. B **784** (2018) 423.

42. Kicińska-Habior, M. *et al.*. Statistical giant dipole resonance decay of highly excited states of ^{63}Cu. Phys. Rev. C **36** (1987) 612.

43. Dey, B. *et al.* Probing the critical behavior in the evolution of GDR width at very low temperatures in A$\sim$100 mass region. Phys. Lett. B **731** (2014) 92.

44. Heckman, P. *et al.*. Low-temperature measurement of the giant dipole resonance width. Phys. Lett. B **555** (2003) 43.

45. Pandit, D., Mukhopadhyay, S., Pal, S., De, A. & Banerjee, S.R. Critical behavior in the variation of GDR width at low temperature. Phys. Lett. B **713** (2012) 434.

46. Wang, M., Huang, W. J., Kondev, F. G., Audi, G. & Naim, S. The AME 2020 atomic mass evaluation (II). Chinese Phys. C **45** (2021) 030003.

Figures

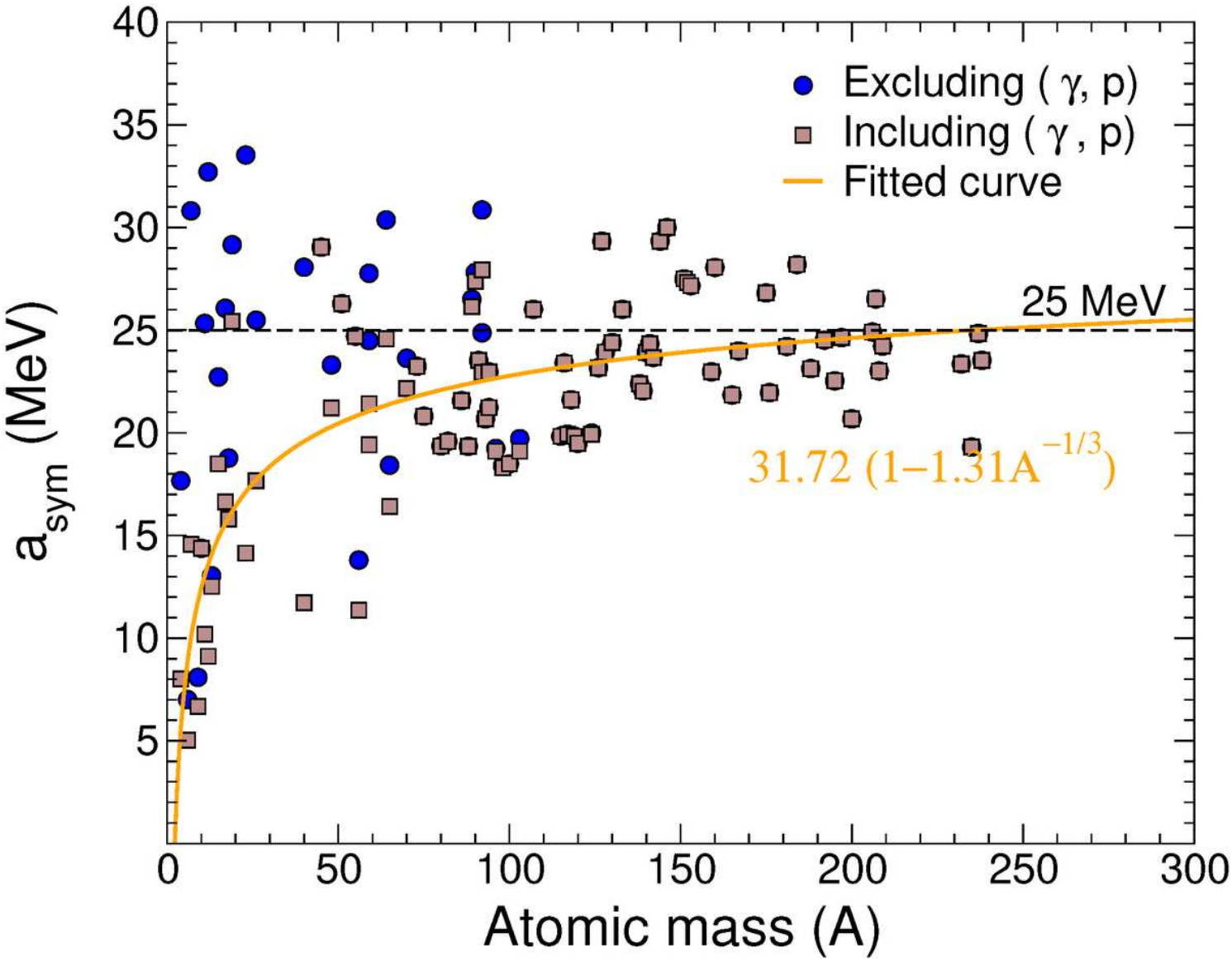

Figure 1

Symmetry energy coefficient, asym(A), of finite nuclei as a function of mass number A extracted from the experimental σ−2 values 36, 37, as given in Eq. 8 and fitted (solid line) by Eq. 2.

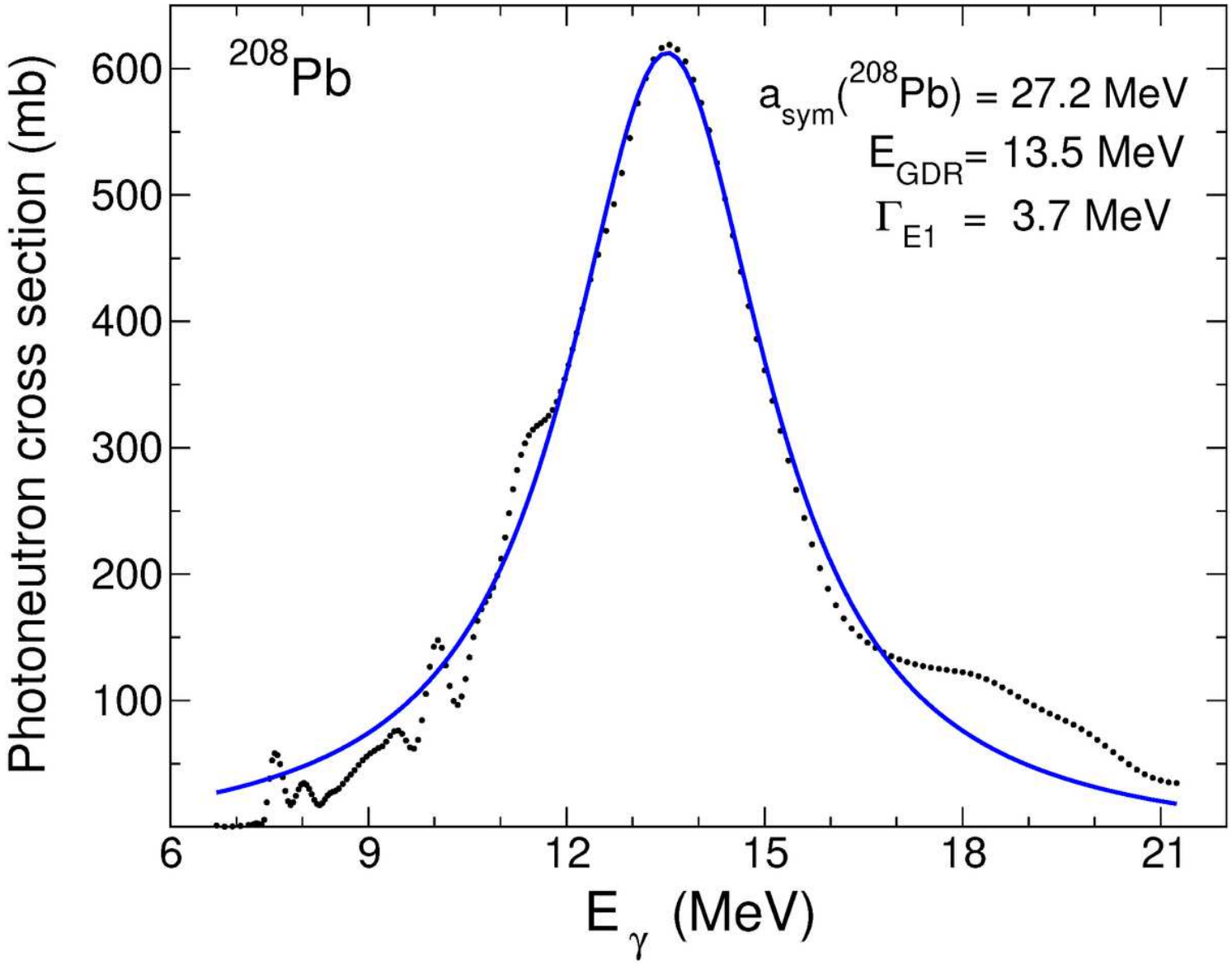

Figure 2

A Lorentzian fit to GDR data extracted for 208Pb 36, 37.

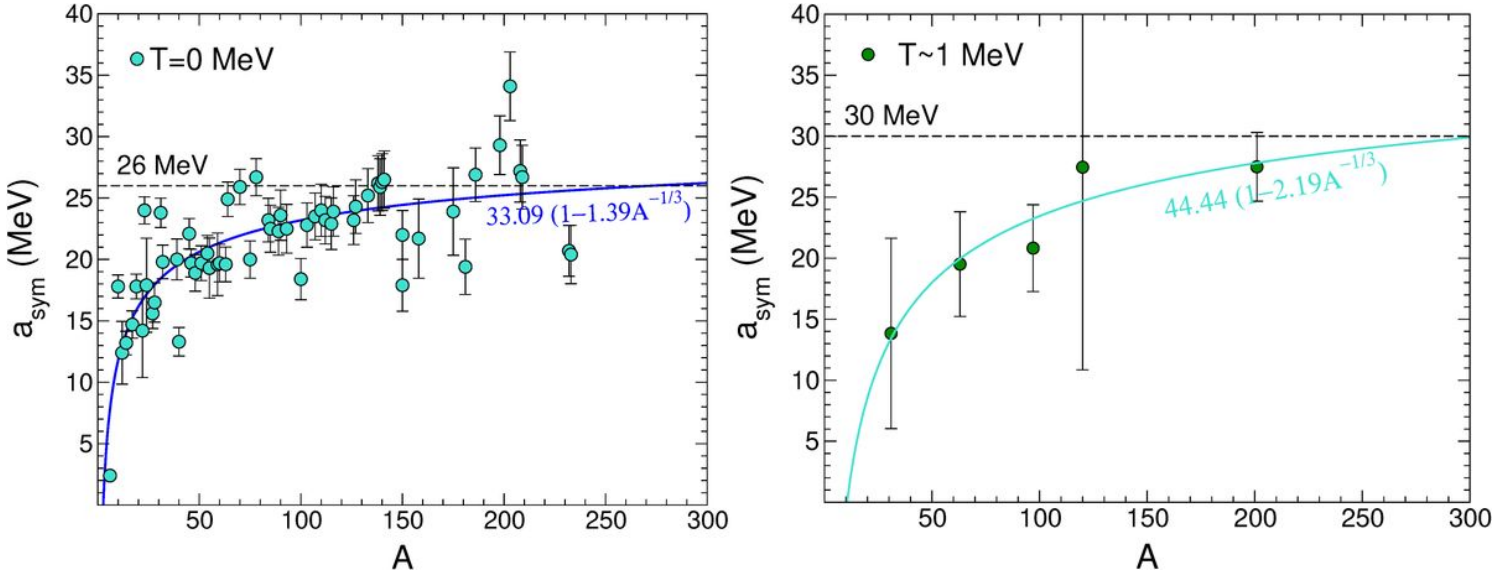

Figure 3

(Color online) Symmetry energy coefficient, asym(A), of finite nuclei as a function of mass number A extracted from GDRs built on ground states (T = 0) (left panel) and excited states (T ≈ 1 MeV) (right panel) using Eqs. 9 and 10.

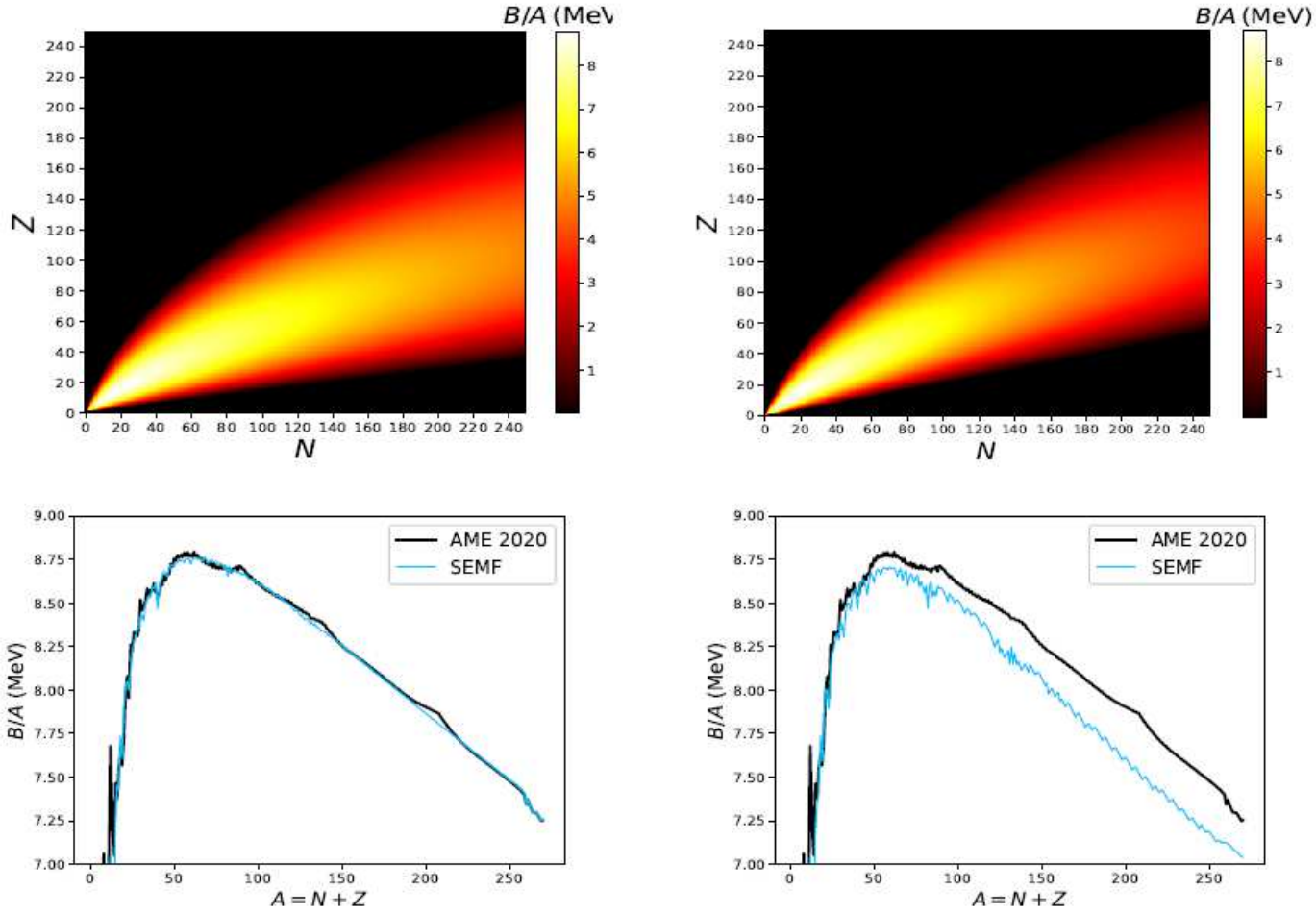

Figure 4

(Color online) Nuclear charts (top panels) and binding energy curves (bottom panels) showing average binding energies per nucleon using the Bethe-Weizs¨acker SEMF for asym = 23 MeV (left) and asym = 30 MeV (right). Atomic masses in the bottom panels are extracted from the 2020 atomic mass evaluation (AME 2020) 46.